NONLINEAR MODELING OF A GUITAR LOUDSPEAKER CABINET

David T. Yeh
Center for Computer Research in Music and Acoustics
Stanford University
Stanford, USA
dtyeh@ccrma.stanford.edu

Balázs Bank
Department of Computer Science
Verona University
Verona, Italy
bank@mit.bme.hu

Matti Karjalainen
Dept. of Signal Processing and Acoustics
Helsinki University of Technology, TKK
Espoo, Finland
matti.karjalainen@tkk.fi

ABSTRACT

Distortion is a desirable effect for sound coloration in electric guitar amplifiers and effect processors. At high sound levels, particularly at low frequencies, the loudspeakers used in classic style cabinets are also a source of distortion. This paper presents a case study of measurements and digital modeling of a typical guitar loudspeaker as a real-time audio effect. It demonstrates the complexity of the driver behavior, which cannot be efficiently modeled in true physical detail. A model with linear transfer functions and static nonlinearity characteristics to approximate the measured behavior is derived based upon physical arguments. An efficient method to simulate radiation directivity is also proposed.

1. INTRODUCTION

Loudspeakers for the electric guitar generally follow the traditional designs from 1950s to 1970s. The loudspeaker cabinets are open- or closed-back designs, and the driver units have a soft, often corrugated paper cone, with relatively stiff suspension, like common loudspeakers of the time. This design clearly deviates from modern Hi-Fi loudspeakers that have a more massive and rigid cone, with less stiff suspension. Such classical drivers have a complicated set of cone breakup modes (resonances) at mid to high frequencies (see [1, 2]), and the natural lowpass characteristics of them are utilized to cut the high-frequency components as needed when playing distorted sound. The inherent nonlinearities and chaotic behavior in guitar loudspeakers are even desired, while in Hi-Fi loudspeakers maximal linearity is the goal.

These properties of classic style guitar loudspeakers make them challenging to model in detail. Often, IIR or FIR filters well approximate the linear characteristics that model the resonances of the cone and the acoustic radiation the cabinet, and have been used in previous amp simulations [3, 4, 5]. Such models are most likely used in commercial modeling amplifiers because they are easy to obtain by measurement in the studio, and easy to implement using standard DSP techniques. In fact, freely available collections of cabinet impulse responses are popular on the internet [6].

Detailed physically-based signal processing models have previously been developed to study the nonlinearities of loudspeakers to linearize them. These lumped models involving numerical integration were implemented for real-time evaluation of design parameters [7], and for a feedback control system [8]. In particular it was found that Volterra models were not sufficient to characterize accurately the nonlinearities of loudspeakers at high amplitudes.

Our measurements corroborate their findings that the behavior of a nonlinear loudspeaker is difficult to model simply. However, it is of great interest to provide the most efficient model that sufficiently replicates the effect of a nonlinear guitar loudspeaker, because typical implementations use very limited hardware resources while providing as many audio effects as possible. Observing that perceptually the nonlinearity at low frequencies is most prominent, we choose to develop and evaluate a simple model suitable for a typical audio effects signal processor. The DSP structure selected comprises a linear transfer function from the electric port to cone vibration, followed by a static (memoryless) nonlinearity, and another linear filter that represents sound radiation from cone vibration.

For this study, we measured and modeled a typical loudspeaker cabinet (Engl 12 inch cabinet, Screamer 50 combo; the amplifier part of the combo was not used), see Fig. 3. The single loudspeaker driver is a Celestion G12 Vintage 30 (30W, 8 Ohm). Section 3 of the paper describes the measurement methodology applied, Section 4 presents fitting of a linear model to the data, Section 5 fitting of a nonlinear model, and Section 6 concludes the paper.

2. BASICS OF LOUDSPEAKER MODELING

Figure 1 depicts the basic structure of a typical open-back guitar loudspeaker cabinet and the construction of the loudspeaker element (driver). A voice coil in a magnetic field moves the diaphragm (cone), which radiates sound, and the movement induces a voltage back to the coil. The cone is suspended at the rim and by a spider in the center. In classical drivers the cone is often corrugated so that, while full piston-like movement happens at low frequencies, toward higher frequencies only a smaller radius of the cone moves together with the voice coil.

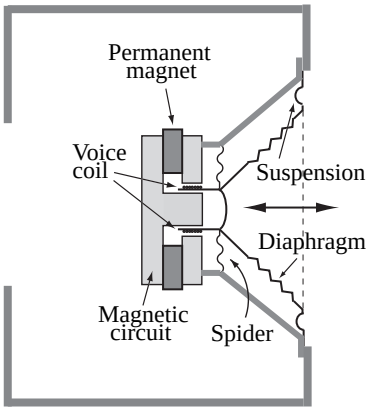

Figure 1: Open-back cabinet and electrodynamic driver.

2.1. Linear behavior

The small-signal behavior of a loudspeaker at low frequencies can be approximated by a lumped element equivalent circuit as shown in Fig. 2 [1]. Here R_e and L_e are the resistance and inductance of the voice coil, and the electric port is driven by power amplifier output voltage e. An ideal transformer with force factor ("turns ratio") of $Bl : 1$ connects the electrical and mechanical subsystems, where B is magnetic field density and l is the length of voice coil in the air gap of the magnet.

The mechanical subsystem in Fig. 2 consists of a mechanical resistance R_m due to velocity-proportional (frictional) losses, suspension compliance C_m, and dynamically moving mass M_m. Load impedance Z_a in Fig. 2 represents acoustic radiation in this mechanical circuit. Cone velocity v multiplied by the cone area yields volume velocity.

At low frequencies the radiated far field sound pressure for a closed enclosure is proportional to the time derivative of volume velocity, or also directly proportional to cone acceleration. In comparison, the open-back cabinet is rather like a dipole radiator, attenuating low frequencies more steeply, but this effect is not as pronounced with close-microphone recording practices. Toward higher frequencies the pressure response should decrease due to the mass of the cone, but the effective area of the cone becomes smaller and the directivity of radiation increases, counteracting these effects to maintain the on-axis response through a comparatively high cutoff frequency for the cone radius, as will be seen from the measurement data.

For a typical loudspeaker, the equivalent circuit is accurate only at low frequencies around the fundamental resonance determined by the mechanical mass and compliance. At frequencies higher than this resonance, the cone can no longer be considered as a rigid mass and should be modeled instead as a distributed system. Wave propagation then explains the many breakup modes, or resonances, of the cone. While in principle the cone could be described as a cylindrical transmission line (waveguide) [2], nonlinearities and chaotic behavior observed in cone vibration make detailed modeling very difficult in practice.

2.2. Nonlinear behavior

The lumped model of Fig. 2 with nonlinear, signal-dependent elements can also describe the low-frequency nonlinear behavior of

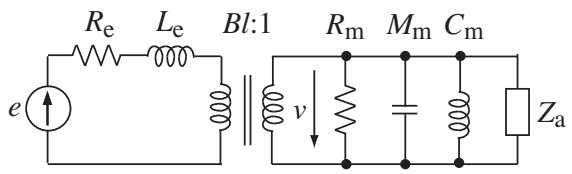

Figure 2: Equivalent circuit of a loudspeaker driver.

the loudspeaker. A concise summary of the comprehensive discussion [9] on the various causes of nonlinearities in loudspeakers follows:

In real loudspeakers, the suspension is not linear but usually increases in stiffness for large displacements. This can be modeled by using a displacement dependent, smoothly saturating function $C_\mathrm{m}(x)$ instead of the the constant C_m. Since the distortion is dependent on x, this effect generates significant distortion only at low frequencies, where displacement is large. Intermodulation distortion is not generated by this effect.

The force factor Bl (the turns ratio of the transformer in Fig. 2) is also a function of coil displacement x, and features a saturating characteristic. At large displacements part of the voice coil leaves the gap, thereby producing less force for the same current i. Notable harmonic distortion is generated only at low frequencies, where cone displacement is large. This phenomenon generates significant intermodulation distortion, which results from amplitude modulation.

The varying voice coil inductance $L_\mathrm{e}(x, i)$ also contributes significantly to the nonlinearity. The electrical impedance at high frequencies is significantly higher for negative displacement than for positive displacement, because the magnet acts like a metal core when the coil is within the magnet structure; outside the magnet, the coil is more like an air core inductor. Additionally, L_e also depends on current, because at high currents the ac magnetic field changes the operating point on the $B(H)$ curve. The varying inductance $L_\mathrm{e}(x, i)$ produces distortion all over the audio band, but its magnitude is generally lower than that generated by $C_\mathrm{m}(x)$ and $Bl(x)$ at low frequencies.

As discussed earlier, the lumped model is only valid for frequencies at which the membrane moves as a rigid body. At higher frequencies, breakup modes appear along with additional nonlinear behavior at large amplitudes. These nonlinearities are caused by geometry changes during the vibration (geometric nonlinearity), and amplitude dependent Young's modulus, E (material nonlinearity). In [10], a nonlinear modal approach models the geometric nonlinearities of a small prototype cone, starting from the Von Kármán plate equations. The flexible corrugated cone of the guitar cabinet presents an even more complicated case and produces notable distortion, as will be seen in the measurements.

3. LOUDSPEAKER CABINET MEASUREMENTS

The first task of the project was to measure the linear and nonlinear behavior of the loudspeaker cabinet. Small-signal measurements characterized the linear properties, while measurements using varying amplitude sine waves as input characterized the nonlinearities. Three different properties were measured: (1) electric port to cone velocity transfer function, (2) electric port to sound pressure radiation, and (3) electric port voltage-current relationships.

3.1. Measurement Setup

A more detailed description of the measurement setup follows:

- *General issues*: Linear input-output relationships were determined by the logarithmic sine sweep technique [11] using the FuzzMeasure software [12] on a Macintosh computer with a Presonus Firepod audio interface. Software written in Pd [13] controlled the distortion measurements for selected frequencies using sine waves with a linearly increasing amplitude ramp. The speaker was driven from a Yamaha MX-70 stereo power amplifier that has low distortion and output impedance.
- *Acoustic response*: The transfer function from electric port voltage to radiated sound pressure was measured in an anechoic chamber, as shown in Fig. 3 using Brüel & Kjær freefield measurement microphones. The near-field response was registered at distance of 10 cm from the dust cap edge on the main axis. Far-field measurements were done at 1.5 m from the cone for horizontal angles of 0, 30, 60, 90, 120, 150, and 180 degrees, and vertically for angles 0, $\pm$30, and 60 degrees.
- *Mechanical response*: The transfer function from electric port voltage to cone velocity was registered by a laser vibrometer (Polytec OFV 303 head and OFV3001 controller) for 6 points, as indicated by the beam reflector tape spots in Fig. 4, starting from P1 at the dust cap edge, radially outward toward the suspension rim position P6. In the figure, the bright point P2 is scattering the beam. We paid special attention to characterization of points P1 and P4. Notice the corrugation of the diaphragm beyond point P3.
- *Electric response*: The impedance of the speaker was measured as the ratio of voltage across and current (converted to voltage in a small resistor in series with the speaker) through the electric port.
- *Nonlinear responses*: Corresponding nonlinearity measurements were done for the transfer properties and electric port behavior with the same hardware and a custom amplitude ramp software. A set of test frequencies was selected: 70 Hz (close to the mechanical resonance of the driver), 100 Hz, 140 Hz, 200 Hz, 400 Hz, 1 kHz, and 4 kHz. The sine sweep ramp duration was two seconds, over which the amplitude increased from zero to a level corresponding to 30 Watts of electric power. For such sweeps, the cone velocity was registered by laser vibrometer, the radiation by the measurement microphone, and the current by a sense resistor at the electric port.

3.2. Measurement Results

The linear electrical impedance of the loudspeaker is shown in Fig. 5. The mechanical resonance frequency $f_0 = 71.2$ Hz and electromechanical quality factor $Q_{\mathrm{TS}} = 0.64$ are determined from the electrical impedance by using Thiele's method [14].

Linear frequency responses of the cone velocity at various radial points are shown in Fig. 6. Note that the mechanical resonance at 71 Hz is present at all the positions shown, confirming piston-like motion at low frequency. This frequency will be used to determine the displacement that influences the nonlinearity. At higher frequency, breakup modes are evident, and these vibrations even affect the center of the cone.

Figure 3: Loudspeaker cabinet in an anechoic chamber for near-field pressure response measurement.

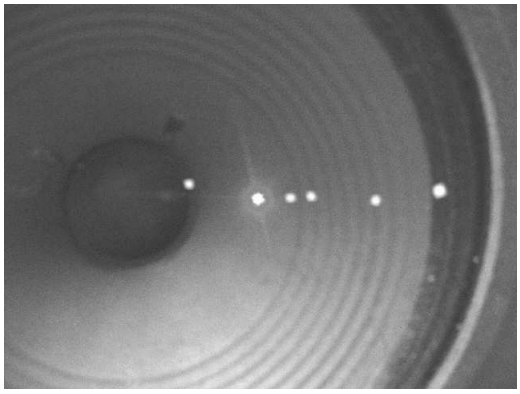

Figure 4: Measurement of cone vibration by laser vibrometer. White spots are reflectors for the laser beam and the bright spot (P2, second from left) is the current scattering point.

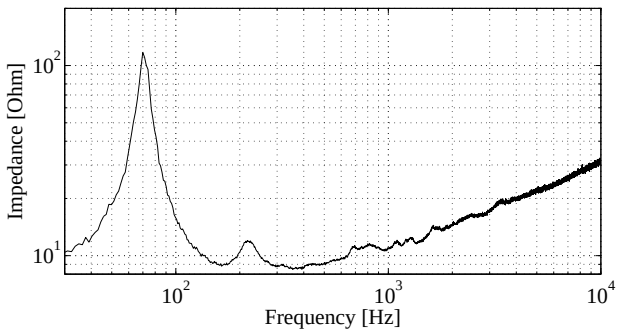

Figure 5: Small signal sweep of loudspeaker electrical port impedance.

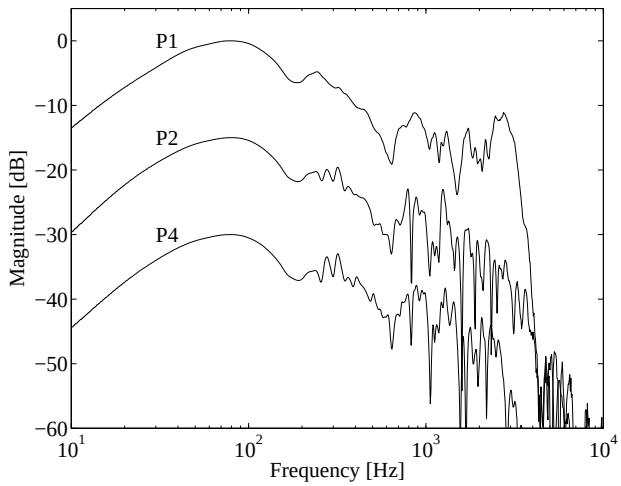

Figure 6: Logarithmic frequency small signal sweep of velocity measured at points P1, P2, and P4, offset for clarity.

	2nd	3rd	4th	5th	THD
70 Hz	-11	-13	-28	-37	-9
100 Hz	-27	-29	-48	-79	-25
140 Hz	-36	-47	-60	-69	-36
200 Hz	-40	-49	-75	-71	-39
400 Hz	-40	-46	-77	-67	-39
4 kHz	-42	-39	-69	-62	-37

Table 1: Distortion in dB, relative to fundamental, of free-field pressure measurement at 0° on axis, 1.5 m distance, 30 W input.

Representative plots of frequency response for small signal pressure measurements are given in Fig. 9 (Sec. 4 on linear modeling) and for distortion as a function of input amplitude in Figs. 13, 14 (Sec. 5 on nonlinear fitting). Much of the salient timbre imparted by the loudspeaker comes from the linear filtering.

Harmonic distortion figures for the frequencies tested are tabulated in Table 1 for an input level corresponding to approximately 30 W, which was noted to sound softer in volume than it typically does for playing at concert levels. This is partially due to the use of single tone sinusoids for the test.

A final oddity of the loudspeaker will be noted here. During the nonlinear test using the amplitude ramp at 1000 Hz, we found that the loudspeaker produced the first subharmonic at high input levels. Figure 7 shows the harmonics as a function of input level for the cone velocity signal. Notice that the subharmonic appears shortly after 1 sec, and is much stronger at P4 than at P1, clearly dominating over the fundamental.

4. LINEAR MODELING

The small-signal behavior of the guitar speaker can be described by a voltage to pressure transfer function. This transfer function includes the vibration of the mechanical system (voice coil, cone) and the radiation effects, and can be implemented as a single digital filter.

The poles of the measured transfer functions generally correspond to break-up modes of the cone. Radiation waves from

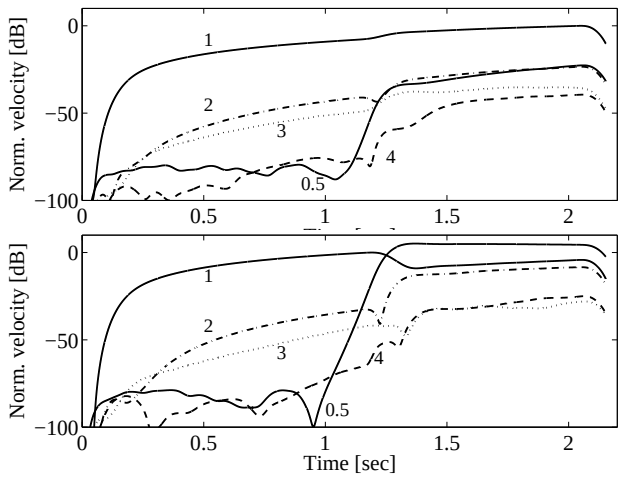

Figure 7: (Sub)-Harmonic distortion products of cone velocity normalized to fundamental strength for linear amplitude ramp at 1000 Hz, points P1 (top), P4 (bottom). Lines 1–4 are fundamental to 4th harmonic, and line 0.5 is subharmonic (500 Hz).

these modes superpose constructively or destructively, depending on their relative phases at the listener, and cause variation in spatial response. This physical interpretation motivates the use of a shared pole set to model transfer functions to different locations.

The fixed-pole parallel second-order IIR filter, also known as the "parallel filter," which was successfully applied to instrument body modeling [15] and loudspeaker-room response compensation [16] in prior work, will model the linear response of the guitar loudspeaker here because it takes into account the logarithmic frequency resolution of hearing to minimize computational complexity.

4.1. Parallel filter formulation

The transfer function of the parallel filter is

$$H(z^{-1}) = \sum_{k=1}^{K} \frac{d_{k,0} + d_{k,1} z^{-1}}{1 + a_{k,1} z^{-1} + a_{k,2} z^{-2}} + \sum_{m=0}^{M} b_m z^{-n}, \quad (1)$$

where K is the number of second order sections, and the second sum constitutes the optional FIR part, which is not used here and will be omitted subsequently. The filter structure is depicted in Fig. 8. Every second-order section of this filter corresponds physically to a specific breakup mode of the cone, and its weights $d_{k,0}, d_{k,1}$ determine its contribution to the radiated sound pressure. However, if the model order is lower than the order of the physical system, the poles do not necessarily correspond to real modes. In particular, the warped Prony's method used for determining the poles attempts to model the overall behavior of the transfer function instead of determining the precise pole locations for a few specific modes.

Because hearing is relatively insensitive to absolute filter phase, the measured impulse responses are first converted to minimum-phase. The poles of the parallel filter are then determined by fitting a warped IIR filter [17] to the transfer function measured on-axis (0°) by using Prony's method. The warped poles

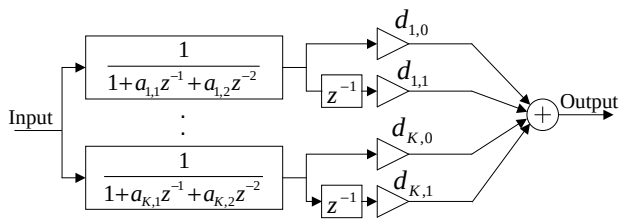

Figure 8: The structure of the parallel second-order filter.

$\tilde{p}_k$ are converted back to linear frequency scale by the expression

$$p_k = \frac{\tilde{p}_k + \lambda}{1 + \tilde{p}_k}, \tag{2}$$

where λ is the warping parameter that was used to design the warped IIR filter. Then, the same pole set is used to fit filters to responses for different angles measured.

Because the poles of the IIR filter are predetermined by Prony's method, (1) becomes linear in its free parameters $d_{k,0}$, $d_{k,1}$, and b_m. We optimize for these free parameters by minimizing the error in the discrete time domain.

The impulse response of the parallel filter is given by

$$h(n) = \sum_{k=1}^{K} d_{k,0} u_k(n) + d_{k,1} u_k(n-1), \tag{3}$$

where $u_k(n)$ is the impulse response of the transfer function $1/(1 + a_{k,1}z^{-1} + a_{k,2}z^{-2})$, which is an exponentially decaying sinusoidal function. Writing (3) in matrix form yields

$$\mathbf{h} = \mathbf{M}\mathbf{p}, \tag{4}$$

where $\mathbf{p} = [d_{1,0}, d_{1,1}, \ldots d_{K,0}, d_{K,1}]^T$ is a column vector composed of the free parameters. The rows of the modeling signal matrix $\mathbf{M}$ contain the direct and delayed impulse responses, $u_k(n)$, and $u_k(n-1)$, of each of the model's parallel filters. Finally, $\mathbf{h} = [h(0) \ldots h(N)]^T$ is a column vector representing the resulting impulse response. The problem reduces to finding the optimal parameters $\mathbf{p}_{\mathrm{opt}}$ that minimize the distance between $\mathbf{h} = \mathbf{M}\mathbf{p}_{\mathrm{opt}}$ and the target response $\mathbf{h}_{\mathrm{t}}$. If the error function is evaluated in the mean squares sense, the optimum is found by the least square (LS) solution

$$\mathbf{p}_{\mathrm{opt}} = (\mathbf{M}^{\mathrm{H}}\mathbf{M})^{-1}\mathbf{M}^{\mathrm{H}}\mathbf{h}_{\mathrm{t}}, \tag{5}$$

where $\mathbf{M}^{\mathrm{H}}$ is the conjugate transpose of $\mathbf{M}$.

Figure 9 displays voltage to pressure transfer functions that model the guitar speaker using 50th and 16th order parallel filters (25 and 8 pole pairs, respectively) for the responses at 0° and 30° in the horizontal plane. The poles determined from the on-axis (0°) response can also successfully model the responses at other locations. From a perceptual point of view, the 16th order model produces good sounding results that impart the timbral effect of the loudspeaker while also smoothing measurement noise. Furthermore, the sonic differences from the 50th order model would be subtle in the typical noisy environment for playing electric guitar.

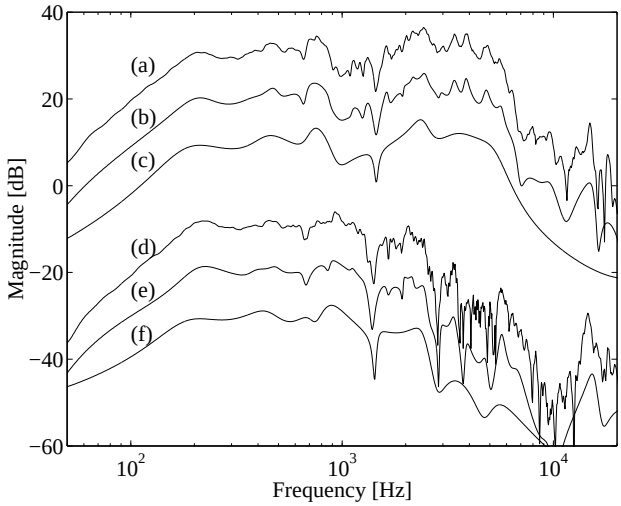

Figure 9: Common pole modeling of the guitar cabinet transfer function using the parallel filter: on-axis measured (a), modeled by a 50th order filter (b), and by a 16th order filter (c). The same pole set is used for modeling the off-axis (30°) response: measured (d), modeled by a 50th order filter (e), and by a 16th order filter (f). The transfer functions are offset for clarity.

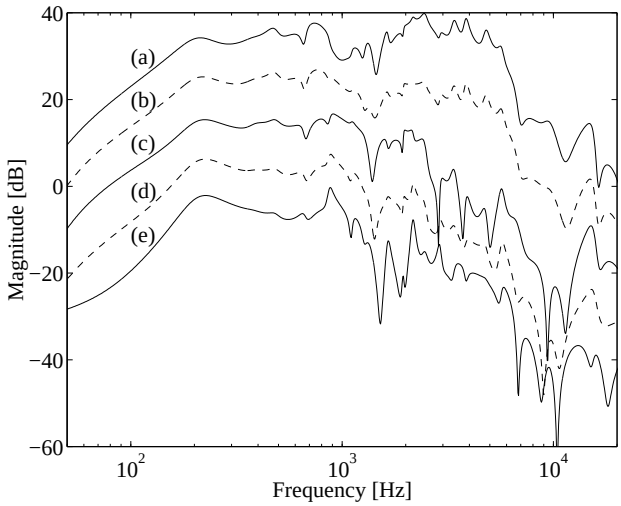

Figure 10: Common pole modeling of the guitar cabinet transfer function using a 50th order parallel filter. Only modeled responses are shown: (a) estimated from the 0° transfer function, (c) from the 30° transfer function, and (e) from the 60° transfer function. The dashed lines show interpolated transfer functions (b) between 0° and 30°, and (d) between 30° and 60°. The curves are offset for clarity.

4.2. Advantages of the parallel filter

The greatest benefit of common pole modeling is that the modeled responses can be efficiently interpolated. Linearly interpolating the $d_{k,0}$, $d_{k,1}$ parameters estimated for different angles corre-

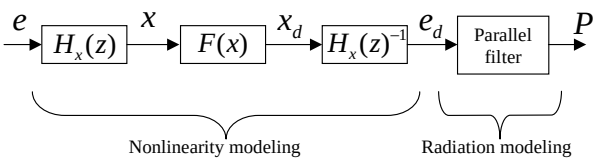

Figure 11: Simplified nonlinear model of the guitar loudspeaker.

sponds to linearly interpolating between the measured responses, analogous to interpolating the parameters of FIR filters. This is depicted in Fig. 10, where the responses at 15° and 45° (dashed lines) are computed by averaging the $d_{k,0}$, $d_{k,1}$ parameters of the responses at 0° and 30°, and 30° and 60°, respectively. This results in a seamless transition without artifacts, in contrast with interpolating between IIR filters with different poles.

Because switching between different angles does not produce transients, this enables interesting effects, such as the sound of the guitar cabinet with a virtual microphone rotating around it at high speed, similar to the Leslie effect discussed in [18]. It is common practice to use multiple microphones to pick up the sound of the cabinet, and mix these signals to achieve the desired tone. In this case only the output coefficients the $d_{k,0}$, $d_{k,1}$ need to be reimplemented, which reduces computational complexity. Another application requiring radiated sound at different angles is simulating the interaction of the guitar cabinet with a virtual room whose reflections are computed by the image-source method.

5. NONLINEAR MODEL FITTING

We will now develop a simple model for the nonlinear effect of the guitar loudspeaker based upon physical arguments.

A computationally efficient model can be made if only the low frequency distortions are considered. We justify this by noting that low frequency nonlinearities dominate the detected distortion in the pressure signal, partly because the fundamental for low frequency signals radiates less efficiently than the distortion products. The total harmonic distortion around the resonance frequency of the speaker is roughly 10%-30% or more, while in the high frequencies it is around 1%, which will be masked by the distortion of the guitar amplifier. We thus assume for this model that a memoryless, or static, nonlinearity characterizes this nonlinear behavior.

The dominant causes of distortion at low frequencies are the nonlinear force factor $Bl(x)$ and the nonlinear compliance $C_\mathrm{m}(x)$, which both depend on the coil displacement x. In this model, a low order polynomial curve approximates the effects of both of these nonlinearities together as a single function mapping linear coil displacement x to a distorted effective cone displacement x_d. Therefore, the overall strategy is to find a transfer function from the input voltage signal e to a linear coil displacement x, compute effective x_d as a polynomial of x, and then convert back to an equivalent distorted input voltage e_d to take advantage of the existing parallel filter, which accounts for radiation effects.

Figure 11 depicts the complete model structure.

5.1. Model development

We assume that the Laplace transform of the voice coil displacement $X(s)$ can be related to the input voltage $E(s)$ of the loudspeaker by the following linear transfer function [14]:

$$H_\mathrm{x}(s) = \frac{X(s)}{E(s)} = K\frac{1}{1+\frac{s}{\omega_0 Q_\mathrm{TS}}+\frac{s^2}{\omega_0^2}}, \tag{6}$$

where $\omega_0 = 2\pi f_0$ is the resonance frequency of the speaker, Q_TS is the total quality factor, s is the Laplace transform variable evaluated at $s = j\omega$, and $K = BlC_\mathrm{m}/R_\mathrm{e}$ is the DC displacement sensitivity depending on the force factor Bl, compliance C_m, and electric resistance R_e. Note that Eq. (6) neglects the high-frequency roll-off due to the inductance L_e of the driver and the high-frequency resonances of the membrane. However, the approximation calculates a sufficiently accurate displacement at low frequencies, where accurate distortion is desired.

The Euler method ($s \to 1 - z^{-1}$) transforms the second-order low-pass filter of Eq. (6) to a digital implementation:

$$H_\mathrm{x}(z) = \frac{K}{1+\frac{1}{\vartheta_0 Q_\mathrm{TS}}+\frac{1}{\vartheta_0^2}+z^{-1}\left(-\frac{1}{\vartheta_0 Q_\mathrm{TS}}-\frac{2}{\vartheta_0^2}\right)+z^{-2}\frac{1}{\vartheta_0^2}}, \tag{7}$$

where $\vartheta_0 = \omega_0/f_\mathrm{s}$ is the discrete-time resonance frequency in radians, and f_s is the sampling frequency.

The resulting linear voice coil displacement x maps to an effective distorted displacement x_d, accounting for the nonlinear effects of $Bl(x)$ and $K(x)$, through a fifth order polynomial:

$$x_\mathrm{d} = F(x) = x + p_2x^2 + p_3x^3 + p_4x^4 + p_5x^5. \tag{8}$$

This effective displacement is physically related to the perceived sound pressure by a linear transfer function. To use the existing parallel filter of Section Sec. 4, which was designed for voltage input, the inverse filter of Eq. (7),

$$H_\mathrm{x}(z)^{-1} = \frac{1}{K}\left[1+\frac{1}{\vartheta_0 Q_\mathrm{TS}}+\frac{1}{\vartheta_0^2}+ z^{-1}\left(-\frac{1}{\vartheta_0 Q_\mathrm{TS}}-\frac{2}{\vartheta_0^2}\right)+z^{-2}\frac{1}{\vartheta}\right], \tag{9}$$

converts the distorted displacement signal x_d to an equivalent distorted voltage e_d. Note that using the Euler method for discretizing Eq. (6) facilitates finding this second-order FIR high-pass inverse. Alternatively using the bilinear transform would be problematic because it produces a zero at the Nyquist frequency for $H_\mathrm{x}(z)$, leading to infinite gain in the inverse filter $H_\mathrm{x}(z)^{-1}$.

5.2. Parameter estimation

The impedance measurement determined the parameters for the displacement filter to be $f_0 = 71.2$ Hz and $Q_\mathrm{TS} = 0.64$. Parameter $K = 0.136$ mm/V was determined from the small signal velocity measurement of the cone for the point P1.

The coefficients $p_2..p_5$ of Eq. (8) are found by fitting the model to the measured distortion products at 70Hz from the nonlinear velocity response at P1. Integrating this velocity measurement determines the displacement response and computes the maximum measured displacement to be 3 mm (6 mm peak-to-peak).

The polynomial fit was performed by comparing plots of the distortion components for the measured and fitted displacement responses to the amplitude ramp as in Fig. 13 and adjusting coefficients manually. The polynomial function matches well to the

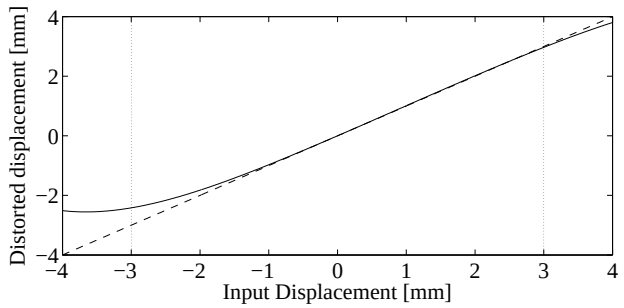

Figure 12: Static nonlinearity $x_{\mathrm{d}} = F(x)$ in the distortion modeling block. The dashed line shows a linear response for comparison, and the vertical dotted lines indicate the limits of parameter fitting.

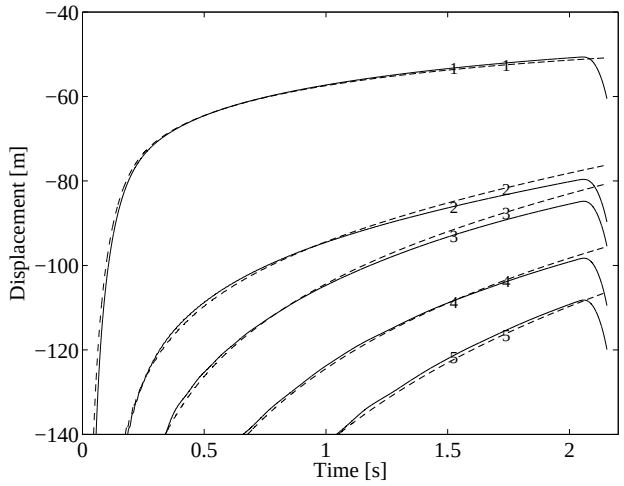

Figure 13: Sinusoidal amplitude ramp at 70 Hz, amplitudes of the distortion terms of the extracted displacement signal: measured (solid line) and modeled (dashed line). The numbers indicate the order of the distortion products, where 1 corresponds to the fundamental, 2 to the second-order distortion, etc.

measurement as plotted in Fig. 13, indicating that the distortions for the range of measured signal levels are weak, and not hard-limiting. The resulting static nonlinearity is displayed in Fig. 12

Because the nonlinearity is not truly memoryless, the model fitted to 70 Hz will be less accurate at other frequencies. Figure 14 compares the model behavior with the measured distorted displacement for the amplitude ramp at 140 Hz. While the model produces higher distortion than measured, the qualitative effect is similar. For frequencies above 400-500 Hz, the model produces negligible distortion because the second-order low-pass filter Eq. (7) attenuates the input to the static nonlinearity, and also keeps aliasing negligible.

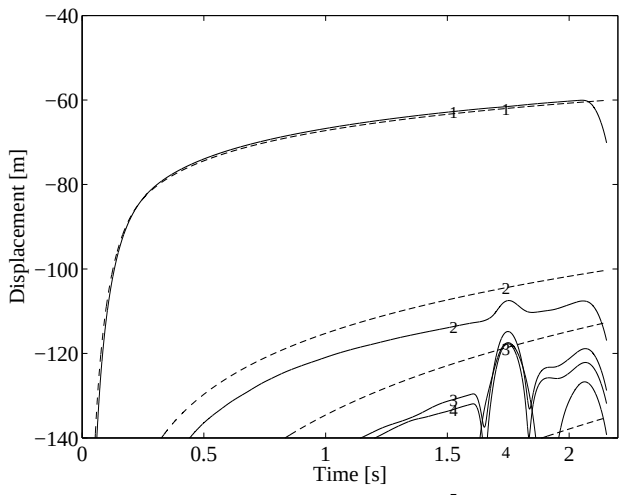

Figure 14: Sinusoidal amplitude ramp at 140 Hz, amplitudes of the distortion terms of the extracted displacement signal: measured (solid line) and modeled (dashed line), with model parameters optimized for the 70 Hz measurement. The numbers indicate the order of the distortion products.

5.3. The complete model

The DSP model for the nonlinear guitar loudspeaker consists of two blocks: a nonlinear processing stage, and the linear parallel filter of Sec. 4.

Figure 15 displays the linear and nonlinear responses of the complete model to a logarithmic frequency sine sweep with a peak amplitude of 22 V. Percentage distortion can be estimated from the intersection of the corresponding solid and dashed/dotted line in the figure.

The distortion is modeled only at low frequencies, as expected. It can be seen that below 100 Hz, the distortion terms outweigh the linear terms, because they are radiated much more efficiently compared to the fundamental. This phenomenon also causes third-order distortion to dominate over second-order at the lowest frequencies.

Sound examples can be found at http://ccrma.stanford.edu/∼dtyeh/cabinet08/.

6. DISCUSSION AND SUMMARY

This work presents the measurements on a typical guitar loudspeaker, and characterizes its linear and nonlinear behaviors, which are very complex in nature. Distortion of the loudspeaker is found to be a significant effect and deserves further study. Efficient DSP models appropriate for musical effects processing were derived to simulate the direction dependent radiation and the basic nonlinear behavior at low frequencies.

The nonlinear modeling can be considered as a first step towards high-quality cabinet modeling, and the limits of this simple nonlinear model should be studied further, including a comparison to the detailed modeling done in the mainstream loudspeaker literature. If computational resources are available and accuracy is at a premium, the more detailed physical models presented in [9]

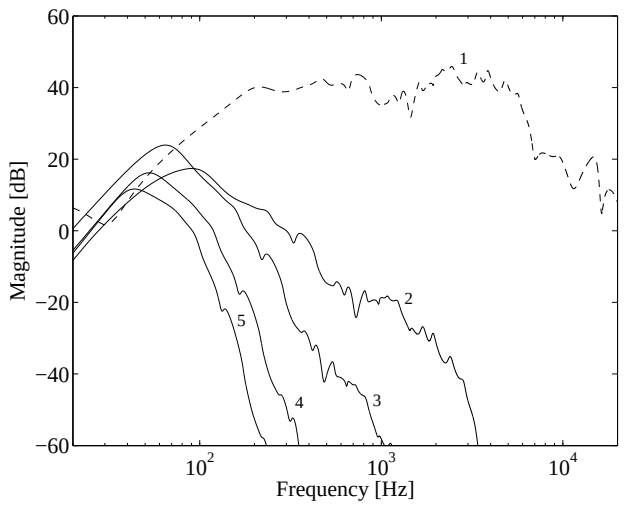

Figure 15: Distortion components of the loudspeaker cabinet model of Fig. 11 as a response to a 22 V amplitude sinusoid of varying frequency. For the parallel filter, the 50th order on-axis model (Fig. 9 (b)) was used. The numbers indicate the order of the distortion products. The fundamental (linear response) is plotted with a dashed line.

should be investigated for future work, and possibly implemented as a wave digital filter [8] for numerical robustness.

Extensions to this work to produce greater realism should account for room effects on the perception of the guitarist. These effects include early reflections and alterations to the frequency response.

The rated limits of a loudspeaker are usually dependent upon the power handling capability of the voice coil. Transient bursts or impulses may momentarily exceed these limits in real playing. The nonlinear transient response of the loudspeaker should also be studied in greater detail.

It is conjectured that for highly distorted input, the distortion of the loudspeaker would be masked. For clean guitar signals with transient or bass content, the distortion could be a significant part of the sound. Formal listening tests should be conducted to assess the audibility of the different distortion components.

7. ACKNOWLEDGMENTS

Special thanks to Jyri Pakarinen and Miikka Tikander for helping in measurements. The work of Balázs Bank in 2007 was supported by a Marie-Curie Intra European Fellowship within the EC 6th Framework Programme contract no. MEIF-CT-2006-041924. David Yeh was supported by the National Science Foundation Graduate Fellowship. This work is also supported by the Academy of Finland project 106956.

8. REFERENCES

[1] L. L. Beranek, *Acoustics*, American Institute of Physics, 1988, Third printing.

[2] M. Colloms, *High-Performance Loudspeakers*, Wiley, 2005, Sixth Edition.

[3] U. Zölzer, *DAFX - Digital Audio Effects*, John Wiley and Sons, 2002.

[4] M. Karjalainen, T. Mäki-Patola, A. Kanerva, and A. Huovilainen, "Virtual Air Guitar," *J. Audio Eng. Soc.*, vol. 54, no. 10, pp. 964–980, 2006.

[5] "CAPS Audio Plugin Suite, 0.4.2 by Tim Goetze," URL: http://quitte.de/dsp/caps.html.

[6] "Noisevault Studio and Convolution Forums," URL: http://noisevault.com/nv/, accessed 17 March 2008.

[7] W. Klippel, "Prediction of speaker performance at high amplitudes," in *Proc. 111th AES Convention*,, New York, USA, Sept. 2001.

[8] D. Fränken, K. Meerkötter, and J. Waßmuth, "Passive Parametric Modeling of Dynamic Loudspeakers," *IEEE Trans. Speech Audio Process.*, vol. 9, no. 8, pp. 885–891, Nov. 2001.

[9] W. Klippel, "Tutorial: Loudspeaker nonlinearities - causes, parameters, symptoms," *J. Aud. Eng. Soc.*, vol. 54, no. 10, pp. 907–939, Oct. 2006.

[10] N. Quaegebeur and A. Chaigne, "Nonlinear modal approach for electrodynamic loudspeaker modeling," in *Proc. Int. Congr. on Acoust.*, Madrid, Spain, Sept. 2007, number MUS-04-004.

[11] Angelo Farina, "Simultaneous measurement of impulse response and distortion with a swept-sine technique," in *Proc. 108th AES Convention*, Paris, France, 2000.

[12] "FuzzMeasure software," URL: http://www.supermegaultragroovy.com/products/FuzzMeasure/.

[13] "Pd, software by Miller Puckett," URL: http://crca.ucsd.edu/∼msp/software.html.

[14] R. H. Small, "Direct-radiator loudspeaker system analysis," *J. Aud. Eng. Soc.*, vol. 20, no. 5, pp. 383–395, Jun. 1972.

[15] B. Bank, "Direct design of parallel second-order filters for instrument body modeling," in *Int. Comp. Music Conf.*, Copenhagen, Denmark, Aug. 2007, pp. 458–465, URL: http://www.acoustics.hut.fi/go/icmc07-parfilt.

[16] B. Bank, "Perceptually motivated audio equalization using fixed-pole parallel second-order filters," *IEEE Sign. Proc. Lett.*, vol. 15, pp. 477–480, 2008.

[17] A. Härmä, M. Karjalainen, L. Savioja, V. Välimäki, U. K. Laine, and J. Huopaniemi, "Frequency-warped signal processing for audio applications," *J. Audio Eng. Soc.*, vol. 48, no. 11, pp. 1011–1031, Nov. 2000.

[18] J. O. Smith, S. Serafin, J. Abel, and D. Berners, "Doppler simulation and the Leslie," in *Proc. COST-G6 Conf. on Digital Audio Effects (DAFx-02)*, Hamburg, Germany, sept 2002, pp. 13–20.